A Journal of the Gesellschaft Deutscher Chemiker

Angewandte International Edition GDCh Chemie

www.angewandte.org

Accepted Article

Title: Stable Heterometallic Cluster-Based Organic Frameworks Catalysts for Artificial Photosynthesis

Authors: Ya-Qian Lan, Long-Zhang Dong, Lei Zhang, Qing Huang, Meng Lu, Wen-Xin Ji, and Jiang Liu

To be cited as: *Angew. Chem. Int. Ed.* 10.1002/anie.201913284
Angew. Chem. 10.1002/ange.201913284

Link to VoR: http://dx.doi.org/10.1002/anie.201913284
http://dx.doi.org/10.1002/ange.201913284

WILEY-VCH

10.1002/anie.201913284

WILEY-VCH

Stable Heterometallic Cluster-Based Organic Frameworks Catalysts for Artificial Photosynthesis

Long-Zhang Dong, Lei Zhang, Jiang Liu*, Qing Huang, Meng Lu, Wen-Xin Ji and Ya-Qian Lan*

Abstract: Coupling CO_2 reduction with H_2O oxidation reactions on one photocatalyst has always been a challenging task in artificial photosynthesis. Herein, we first report a series of stable heterometallic Fe_2M cluster-based MOFs (**NNU-31-M**, M = Co, Ni, Zn) photocatalysts, which can achieve the overall conversion of CO_2 and H_2O to HCOOH and O_2 without the assistance of additional sacrificial agent and photosensitizer. The heterometallic cluster units and photosensitive ligands excited by visible light generate separated electrons and holes. Then, low-valent metal M accepts electrons to reduce CO_2, and high-valent Fe uses holes to oxidize H_2O. This is the first MOF photocatalyst system to finish artificial photosynthetic full reaction. It is noted that **NNU-31-Zn** exhibits the highest HCOOH yield of 26.3 μmol g^{-1} h^{-1} (selectivity of *ca*. 100%). Furthermore, the DFT calculations based on crystal structures demonstrate the photocatalytic reaction mechanism. This work proposes a new strategy for how to design crystalline photocatalyst to realize artificial photosynthetic overall reaction.

In recent years, increasing anthropogenic CO_2 emissions have caused severe energy and environmental issues[1]. In response to these problems, a large number of research works had concentrated on exploring effective ways to achieve the artificial conversion of CO_2[2]. Inspired by plant photosynthesis, which uses solar energy to convert CO_2 and H_2O into carbohydrates and O_2, it is hoped that CO_2 can be reduced in H_2O to high value-added chemicals or fuels by artificial photosynthesis.[3] However, considering the inherent chemical inertness of CO_2 and slow reaction kinetics, effective combination of CO_2 reduction and H_2O oxidation half-reactions (i.e. overall reaction) in one photocatalytic system is still a daunting work. At present, the overall reaction could be achieved by a few nanostructured photocatalysts such as Z-scheme heterojunctions (e.g., Cu_2O/WO_3[4] and α-Fe_2O_3/Cu_2O[5]). However, because of the influences of defects, impure phases and complicated structural components, there is still lack of sufficient and clear structural information to identify the specific catalytic sites in these catalysts. Thus, exploring crystalline photocatalytic system with well-defined structure is considered as one of the most promising choices to address these issues.[6]

The crystalline heterometallic cluster has the potential to perform artificial photosynthetic overall reaction, because of their two advantages. On the one hand, the heterometallic cluster can simultaneously bear the active catalytic sites of CO_2 reduction and H_2O oxidation half-reactions and possess accurate structural information. On the other hand, the heterometallic cluster can gather and provide multi-electron transfer[7] for photocatalytic reactions, and increase the synergistic effect of oxidative and reductive active sites[8]. However, heterometallic cluster serving as photocatalyst still faces many problems such as poor water stability, low specific surface area and CO_2 adsorption ability. In particular, the molecular cluster catalysts are hard to separate from reaction solution due to their homogeneous nature.[9] In this regard, a lot of metal-organic framework (MOF) photocatalysts have recently been explored to solve above problems, and some of them have excellent performance on CO_2 photoreduction.[10] But all these works, the use of additional sacrificial agents in the reaction has not been solved yet. Thus, if the heterometallic cluster molecules can be assembled with photosensitive organic linkers to construct stable heterometallic cluster-based MOFs that will further extend their photocatalytic advantages such as i) improving the visible light absorption and structural stability; ii) facilitating the utilization of photogenerated electrons and holes (due to the near electron-hole transport distance); iii) increasing CO_2 adsorption by porosity and exposing more active sites to activate CO_2 and H_2O molecules; iv) studying photocatalytic reaction mechanism by their well-defined structures to provide more insights into structure-property correlations. Based on these advantages, we believe that the construction of stable heterogeneous heterometallic cluster-based MOF photocatalysts is a promising strategy for the realization of artificial photosynthetic overall reaction.

With this thought in mind, we chose the stable $Fe_2M(\mu_3\text{-}O)(OAc)_6(H_2O)_3$ (Fe_2M, M= Co, Ni, Zn) clusters[11] and photosensitive 4,4',4''-tricarboxytriphenylamine (TCA) ligand to construct three stable heterometallic cluster-based MOFs, $[Fe_2M(\mu_3\text{-}O)(TCA)_2(H_2O)_3]$ (**NNU-31-M,** M = Co, Ni, Zn), which are expected to display above-mentioned advantages. Within these structures, high-valent Fe^{3+} and low-valent M^{2+} ions are considered to play the roles of oxidation and reduction active sites, respectively, while the TCA ligand and heterometallic cluster itself are used for visible-light absorption. As expected, **NNU-31-M** successfully achieve the CO_2 reduction coupled with H_2O oxidation without adding additional photosensitizers and sacrificial agents. Among them, **NNU-31-Zn** showed the highest HCOOH yield rate of 26.3 μmol g^{-1} h^{-1} and high selectivity (~100%). The DFT calculation results indicate that the CO_2 reduction reaction (CO_2RR) is more likely to occur on Zn, and the Fe is more susceptible to the H_2O oxidation reaction. Significantly, this is the first report of MOF system as photocatalysts to finish artificial photosynthetic overall reaction, thus it brings more opportunities for designing crystalline photocatalysts to reduce CO_2 with H_2O.

[*] L.-Z. Dong, L. Zhang, Dr. J. Liu*, Q. Huang, M. Lu and Prof. Y.-Q. Lan*
Jiangsu Collaborative Innovation Centre of Biomedical Functional Materials, Jiangsu Key Laboratory of New Power Batteries, School of Chemistry and Materials Science
Nanjing Normal University
No. 1, Wenyuan Road, Nanjing, 210023 (China)
E-mail: liuj@njnu.edu.cn
yqlan@njnu.edu.cn
Dr. W.-X Ji
State Key Laboratory of High-efficiency Coal Utilization and Green Chemical Engineering
Ningxia University
Yinchuan, 750021 (China)

10.1002/anie.201913284

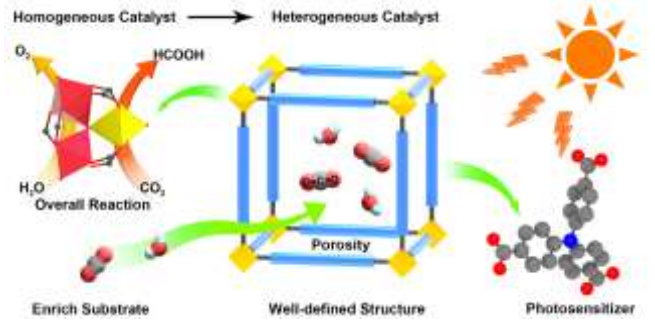

Sheme 1. Functions of the heterometallic cluster-based organic framework as photocatalyst

NNU-31-M were synthesized by the TCA ligands and prefabricated Fe_2M clusters under solvothermal condition.[11a] The **NNU-31-Zn** is black elongated square bipyramid single crystal. X-ray single-crystal diffraction indicated that **NNU-31-Zn** crystallizes in the orthorhombic system with a $Pca2_1$ space group (Table S1). Moreover, the powder X-ray diffraction (PXRD) patterns of **NNU-31-Co** and **NNU-31-Ni** are identical to **NNU-31-Zn**, demonstrating that **NNU-31-M** MOFs are isostructural. There are two Fe^{3+} ions, one M^{2+}, one μ_3-O, six OAc^- groups and three H_2O molecules in Fe_2M cluster (Figure S1). The asymmetric unit of **NNU-31-Zn** contains four TCA ligands, four Fe^{3+} ions, two Zn^{2+} ions, two μ_3-O^{2-} and six H_2O molecules (Figure S2). The six OAc^- of the cluster were completely replaced by the carboxyl groups from the TCA, and each TCA ligand links to three Fe_2M clusters (Figure S3). By these connection modes, the three-dimensional (3D) framework and channels of **NNU-31-M** are shown as Figure 1a and 1b. In addition, topological analysis by TOPOS[12] shows **NNU-31-Zn** is a 3,6-c net topology (Schläfli symbol as $\{4\cdot6^2\}\{4\cdot6^9\cdot8^5\}\{6^3\}$). The tilling of **NNU-31-Zn** is shown in Figure 1c, and its free volume is calculated to be 68.5% by PLATON[13] software.

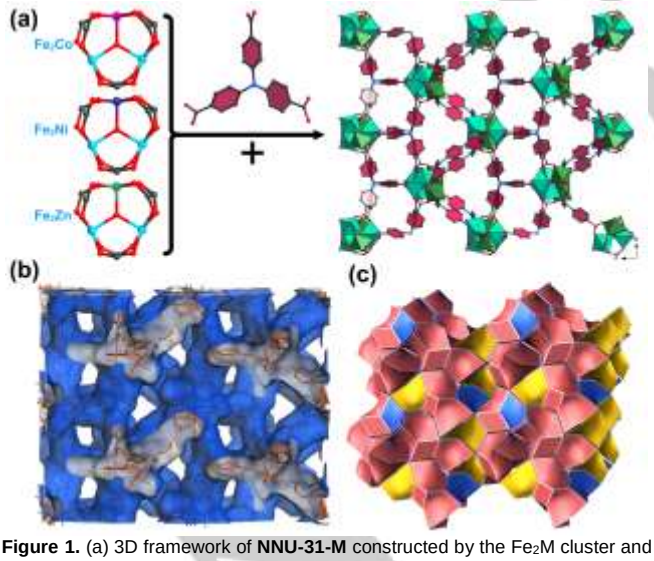

Figure 1. (a) 3D framework of **NNU-31-M** constructed by the Fe_2M cluster and TCA. (b) 3D channel simulated diagram of **NNU-31-Zn**. (c) The tilling of **NNU-31-Zn**.

The PXRD patterns of the synthesized **NNU-31-M** were in good agreement with the simulated pattern from single-crystal X-ray diffraction (Figure 2a), indicating that they have fine crystallinity and high purity. To evaluate the water stability of **NNU-31-M**, 20 mg crystals were immersed into 100 mL water at room temperature for several days. The consistent PXRD patterns affirmed that **NNU-31-M** MOFs possess good water stability (Figure S4). According to both energy dispersive spectrometer (EDS) (Figure S5, Table S2) and inductively coupled plasma atomic emission spectroscopy (ICP-AES) results (Table S3), the stoichiometric ratios of Fe/M in **NNU-31-M** are 2:1. The thermogravimetric analysis (TGA) indicated that **NNU-31-M** MOFs have high thermal stability (Figure S6). The N_2 adsorption–desorption isotherms displayed in Figure S7 were typical type-I isotherm with a sharp N_2 uptake at low relative pressure, and the corresponding pore-size distributions were showed in Figure S8. Meanwhile, the CO_2 adsorption isotherms of **NNU-31-M** were measured at 298 K and under 1 atm and estimated to be 24.01 (Co), 29.66 (Ni) and 36.97 (Zn) $cm^3\ g^{-1}$ (Figures S9-S10), respectively.

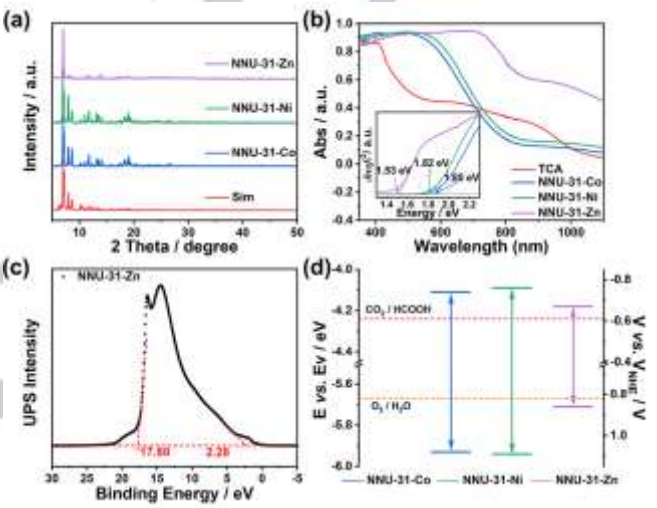

Figure 2. (a) PXRD patterns of **NNU-31-M**. (b) UV-Vis-NIR DRS spectra of **NNU-31-M** and tauc plot for bandgap calculation of **NNU-31-M** as inset picture. (c) UPS spectra of **NNU-31-Zn**. (d) Band structure for **NNU-31-M**.

As suggested by the UV-Vis-NIR diffuse reflectance spectroscopy (UV-Vis-NIR DRS) results, the strong visible light absorption of **NNU-31-Co** and **NNU-31-Ni** only extends to ~570 nm and ~590 nm (Figure 2b). By contrast, **NNU-31-Zn** shows a much broader light absorption range (across the entire UV-visible region) than **NNU-31-Co**, **NNU-31-Ni** and free TCA ligand (Figure 2b). It also means that electrons of **NNU-31-Zn** are more easily excited under visible light irradiation than free TCA, **NNU-31-Co** and **NNU-31-Ni**. The bandgaps (E_g) of **NNU-31-M** are determined to be 1.85 (Co), 1.82 (Ni), 1.53 (Zn) eV by their tauc plots (Figure 2b inset)[14], indicating that they have the characteristics of the semiconductor. The ionization potential (equivalent to valence band maximum, VBM) of **NNU-31-M** was determined by ultraviolet photoelectron spectroscopy (UPS), from which the VBM of **NNU-31-Zn** was estimated to be -5.71 eV (*vs.* vacuum level, Ev) by subtracting the excitation energy of 21.22 eV from the width of the He I UPS spectrum (Figure 2c).[15] Likewise, the VBMs of **NNU-31-Co** and **NNU-31-Ni** were determined to be -5.93 and -5.94 eV (*vs.* Ev), respectively (Figures S11-S12). By performing UV-Vis-NIR DRS associated with UPS, the conduction band minimums (CBMs) of **NNU-31-M** MOFs were estimated to be -4.08 (Co), -4.12 (Ni) and -4.18 eV (Zn) (*vs.* Ev), respectively. And the calculated energy-band alignment results are presented in Figure 2d. To verify the accuracy of these results, Mott-Schottky electrochemical measurements were further performed to determine the energy band positions of the semiconductor-like **NNU-31-M** MOFs.

Since the gap between flat band potential and CBM is negligible for n-type semiconductors, the CBM positions of the **NNU-31-M** were determined to be -0.75 (Co), -0.74 (Ni) and -0.67 (Zn) V (*vs.* NHE, pH = 7), respectively (Figures S13-S15). And the VBM positions of the **NNU-31-M** were determined to be 1.10 (Co), 1.08 (Ni) and 0.96 (Zn) V (*vs.* NHE, pH = 7) associated with UV-Vis-NIR DRS (Figures 2c). These results also agree with the values obtained from UPS. Obviously, the CBMs of **NNU-31-M** are more negative than the redox potentials of most photocatalytic reductive products such as HCOOH, CO, etc.,[16] while their VBMs are more positive than the redox potential of O_2/H_2O (0.82 V *vs.* NHE, pH = 7 and -5.67 eV *vs.* Ev)[15]. Therefore, theoretically these MOFs may serve as efficient photocatalysts to performing artificial photosynthetic overall reaction due to the matched band structures. From the photoluminescence (PL) spectra of **NNU-31-M** (Figure S16), the TCA ligand shows an obvious fluorescence emission spectrum centered at 440 nm when excited at 340 nm. However, **NNU-31-M** shows very weak PL signals near 440 nm close to the fluorescence quenching, suggesting the electron transfer between the excited TCA ligand and the cluster unit. To further investigate the differences on photocatalytic activity of these potential MOF photocatalysts, the photocurrent response test was conducted to evaluate photoinduced electron transfer efficiency. Photocurrent response results showed that the photocurrent response of **NNU-31-Zn** is stronger than that of **NNU-31-Co** and **NNU-31-Ni** (Figure S17). Thus, the photogenerated electron-hole pairs in **NNU-31-Zn** can be more efficiently separated by the ligand-metal charge transfer effect.

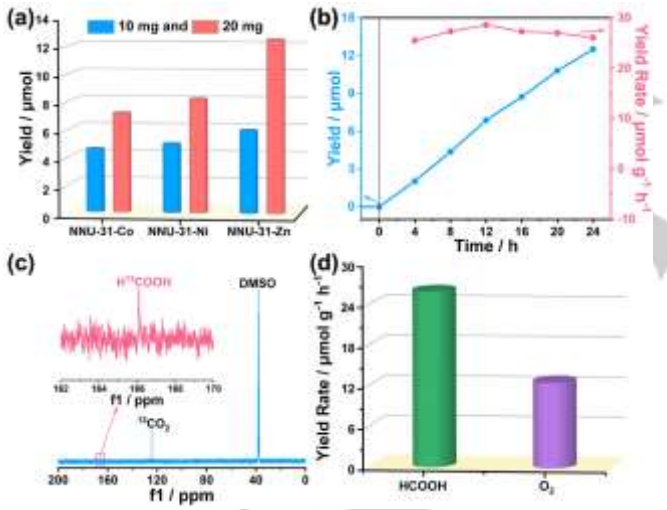

Figure 3. (a) The yield of HCOOH produced with **NNU-31-M** after 24 hours (catalyst weight of 10 or 20 mg). (b) The amount (blue) and production rate (orange) of HCOOH as a function of the time of of visible light irradiation over **NNU-31-Zn**. (c) ^{13}C NMR spectra for reaction solution from with $^{13}CO_2$ atmosphere. (d) The production rates of HCOOH and O_2 in **NNU-31-Zn**.

The visible-light photocatalytic CO_2RR was conducted under pure CO_2 atmosphere in aqueous solution, without the presence of additional photosensitizer and sacrificial agents. As shown in Figure 3a, **NNU-31-Zn** shows the highest HCOOH yield of 12.51 μmol under visible light irradiation after 24 h, which is higher than that of **NNU-31-Co** (7.17 μmol) and **NNU-31-Ni** (8.22 μmol). The amount of HCOOH is determined by ion chromatography (IC) (Figures S18-19). The HCOOH yield increases almost linearly with the irradiation time of the **NNU-31-Zn** catalyst (Figure 3 b). Furthermore, $^{13}CO_2$ isotope experiment was performed to confirm the source of Carbon. As shown in Figure 3c, when $^{13}CO_2$ was employed in the reaction system, a clear peak appeared at 166.4 ppm in the ^{13}C NMR spectrum corresponding to $H^{13}COOH$[10b], which strongly indicates that the produced HCOOH originates from CO_2. When $^{12}CO_2$ was employed in the reaction system, the ^{13}C NMR spectrum has no signal, as shown in Figure S20. At the same time, the production of O_2 was detected by the online test, which was to eliminate the effect of air leakage caused by manual injections (Figure 3 d and Figures S21-22). As expected, the detected HCOOH/O_2 ratio is close to 2:1. Moreover, we also conducted a series of control experiments with **NNU-31-Zn** as an example (Figure S23 and Table S4) to confirm the photocatalytic CO_2RR activity of **NNU-31-M**. The effects of sacrificial donors and hole scavenger on the CO_2 reduction and H_2O oxidation half-reactions of **NNU-31-Zn** were also performed, respectively (Table S5-S6). After photocatalytic reaction, only HCOOH as liquid reduction product could be detected by IC (Figure S18) and ^1H NMR (Figure S24), and O_2 as oxidation product (except trace gaseous reductive products) was detected by GC (Figure S21 and S25), indicating high HCOOH selectivity (~100%) of these MOF-based photocatalysts. The oxygen source of oxidation product (O_2) was also checked by isotopic labelling experiment, in which $^{18}O_2$ (m/z=36) and $^{18}O^{16}O$ (m/z=34) were detected by GC-MS after the reaction using $H_2{}^{18}O$ as the reaction solvent (Figure S26), confirming that the generated O_2 was derived from the H_2O oxidation.

Additionally, this photocatalytic experiment can be recycled for at least three times (Figure S27), and the solution after reaction was detected by inductively coupled plasma mass spectrometry (ICP-MS). It shows that only less than 0.8% of the catalyst is dissolved (Table S7). PXRD, FTIR and XPS characterizations after reaction also proved that **NNU-31-Zn** has good structural stability (Figure S28-30). As shown in Figure S31, the SEM images of these MOFs indicated that the morphologies of the grinded catalysts powders before and after long-term (72 h) photocatalytic reaction are very similar. All the experimental results indicate that **NNU-31-Zn** is an effective and selective heterogeneous photocatalyst to integrate CO_2 reduction and H_2O oxidation half-reactions. Based on the above experiments and analysis, a possible mechanism for explaining CO_2 reduction and H_2O oxidation processes is proposed (Figure 4a). The heterometallic clusters and ligands are excited by visible-light to generated electron-hole pairs. Then electrons are transferred to a low-valent metal to undergo CO_2 reduction, while holes move to high-valent Fe to perform H_2O oxidation.

Density functional theory (DFT) and time-dependent DFT (TDDFT) computational ways were used to explain the photoexcitation process and the catalytic reaction mechanism. The model structures established in the calculation were shown in Figure S32. Since the photo-absorption efficiency plays a key role in the photocatalytic process, we first compare the photo-absorptions of **NNU-31-Zn** and **NNU-31-Ni**, which are shown in Figure 4b. The simulated light absorption of the two systems agrees well with the experiments, a broad spectrum in the range of 550 to 650 nm is clearly identified for **NNU-31-Zn**, while the **NNU-31-Ni** shows very poor absorption in the area. The prominent photo-absorption efficiency of Zn-containing MOFs in the visible light range is attributed to the effective charge transfer from the TCA ligands to the transition metal centers, thus promoting further photocatalytic reactions. In the following, the catalytic reaction mechanisms of CO_2RR and water oxidation on

NNU-31-Zn are investigated by free energy calculations. The conversion from CO_2 to HCOOH requires two hydrogenation processes, from *CO_2 to *OCOH and from *OCOH to *HCOOH, where the first one serves as rate-determining step (RDS). As shown in Figure 4c, the energy barrier of the RDS on the Zn site is slightly preferred over the Fe site, establishing another advantage of **NNU-31-Zn** for photocatalyst. As for water oxidation process, the Fe sites are identified and the dissociation of *OH into O group (*O) with an energy barrier of 2.06 eV is proved to be the potential-determining step for the whole four steps (Figure 4d). The energy barrier of other three steps, the adsorption of an OH group (*OH) that dissociated from a water molecule, the formation of an OOH group (*OOH) by the reaction between *O and anther H_2O, and the generation of O_2, are calculated to be, respectively. Therefore, the overpotential of OER can be obtained by analyzing the reaction free energy of each elementary step, and the calculated η is 0.83 V.

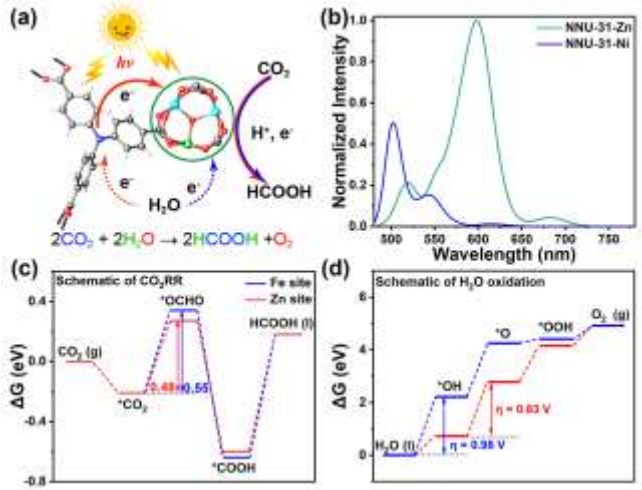

Figure 4. (a) Schematic of the mechanism of **NNU-31-M** CO_2RR with H_2O oxidation. (b) Theoretical simulation light absorption of **NNU-31-Zn** and **NNU-31-Ni**. The free energy profile for the CO_2RR pathway and (c) OER pathway (d).

In summary, a series of stable heterometallic Fe_2M cluster-based MOFs are for the first time used as effective photocatalysts to achieve artificial photosynthetic overall reaction (coupling CO_2 reduction with H_2O oxidation) in the absence of additional sacrificial agent and photosensitizer. Among these photocatalysts, **NNU-31-Zn** shows the highest efficiency for CO_2-to-HCOOH conversion (26.3 μmol g^{-1} h^{-1}) and selectivity of *ca.* 100%. The corresponding DFT calculation results indicate that CO_2RR is more likely to occur on metal Zn, and H_2O oxidation reaction occurs on metal Fe. By constructing these stable crystalline heterometallic cluster-based MOF photocatalysts for artificial photosynthesis, more direct and clear evidence on the structure-function relationship of the photocatalyst is displayed. Significantly, this work can serve as an important case study for designing crystalline photocatalyst to realize artificial photosynthetic overall reaction.

Acknowledgements

This work was financially supported by NSFC (No. 21622104, 21701085, 21871141, 21871142 and 21901122); the NSF of Jiangsu Province of China (No. BK20171032); the Natural Science Research of Jiangsu Higher Education Institutions of China (No. 17KJB150025 and 19KJB150011) and Project funded by China Postdoctoral Science Foundation (No. 2018M630572 and 2019M651873); The East-West Cooperation Project of Ningxia Key R & D Plan (2019BFH02014); Priority Academic Program Development of Jiangsu Higher Education Institutions and the Foundation of Jiangsu Collaborative Innovation Center of Biomedical Functional Materials.

Keywords: heterometallic photocatalyst • carbon dioxide reduce reaction • water oxide • metal-organic framework

[1] a) S. J. Davis, K. Caldeira, H. D. Matthews, *Science* **2010**, *329*, 1330-1333; b) M. Mikkelsen, M. Jørgensen, F. C. Krebs, *Energy Environ. Sci.* **2010**, *3*, 43-81; c) J. Ran, M. Jaroniec, S.-Z. Qiao, *Adv Mater* **2018**, *30*, 1704649.
[2] a) X. Liu, S. Inagaki, J. Gong, *Angew. Chem. Int. Ed.* **2016**, *55*, 14924-14950; b) A. Vasileff, X. Zhi, C. Xu, L. Ge, Y. Jiao, Y. Zheng, S.-Z. Qiao, *ACS Catal.* **2019**, *9*, 9411-9417; c) J. Ran, J. Qu, H. Zhang, T. Wen, H. Wang, S. Chen, L. Song, X. Zhang, L. Jing, R. Zheng, S.-Z. Qiao, *Advanced Energy Materials* **2019**, *9*, 1803402.
[3] a) W. Kim, B. A. McClure, E. Edri, H. Frei, *Chem. Soc. Rev.* **2016**, *45*, 3221-3243; b) M. Lu, J. Liu, Q. Li, M. Zhang, M. Liu, J.-L. Wang, D.-Q. Yuan, Y.-Q. Lan, *Angew. Chem. Int. Ed.* **2019**, *58*, 12392-12397.
[4] W. Shi, X. Guo, C. Cui, K. Jiang, Z. Li, L. Qu, J.-C. Wang, *Appl. Catal. B-Environ.* **2019**, *243*, 236-242.
[5] J.-C. Wang, L. Zhang, W.-X. Fang, J. Ren, Y.-Y. Li, H.-C. Yao, J.-S. Wang, Z.-J. Li, *ACS Appl. Mater. Inter.* **2015**, *7*, 8631-8639.
[6] M. Ding, R. W. Flaig, H.-L. Jiang, O. M. Yaghi, *Chem. Soc. Rev.* **2019**, *48*, 2783-2828.
[7] N. A. Vante, H. Tributsch, *Nature* **1986**, *323*, 431-432.
[8] P. Buchwalter, J. Rosé, P. Braunstein, *Chem. Rev.* **2015**, *115*, 28-126.
[9] a) N. Pinault, D. W. Bruce, *Coordin. Chem. Rev.* **2003**, *241*, 1-25; b) S. Berardi, S. Drouet, L. Francàs, C. Gimbert-Suriñach, M. Guttentag, C. Richmond, T. Stoll, A. Llobet, *Chem. Soc. Rev.* **2014**, *43*, 7501-7519.
[10] a) H.-Q. Xu, J. Hu, D. Wang, Z. Li, Q. Zhang, Y. Luo, S.-H. Yu, H.-L. Jiang, *J. Am. Chem. Soc.* **2015**, *137*, 13440-13443; b) D. Wang, R. Huang, W. Liu, D. Sun, Z. Li, *ACS Catal.* **2014**, *4*, 4254-4260; c) K. M. Choi, D. Kim, B. Rungtaweevoranit, C. A. Trickett, J. T. D. Barmanbek, A. S. Alshammari, P. Yang, O. M. Yaghi, *J. Am. Chem. Soc.* **2017**, *139*, 356-362; d) Q. Huang, J. Liu, L. Feng, Q. Wang, W. Guan, L.-Z. Dong, L. Zhang, L.-K. Yan, Y.-Q. Lan, H.-C. Zhou, *Natl. Sci. Rev.* **2019**; e) N. Li, J. Liu, J.-J. Liu, L.-Z. Dong, Z.-F. Xin, Y.-L. Teng, Y.-Q. Lan, *Angew. Chem. Int. Ed.* **2019**, *58*, 5226-5231.
[11] a) D. Feng, K. Wang, Z. Wei, Y.-P. Chen, C. M. Simon, R. K. Arvapally, R. L. Martin, M. Bosch, T.-F. Liu, S. Fordham, D. Yuan, M. A. Omary, M. Haranczyk, B. Smit, H.-C. Zhou, *Nat. Commun.* **2014**, *5*, 5723; b) X.-L. Wang, L.-Z. Dong, M. Qiao, Y.-J. Tang, J. Liu, Y. Li, S.-L. Li, J.-X. Su, Y.-Q. Lan, *Angew. Chem. Int. Ed.* **2018**, *57*, 9660-9664.
[12] E. V. Alexandrov, V. A. Blatov, A. V. Kochetkov, D. M. Proserpio, *CrystEngComm* **2011**, *13*, 3947-3958.
[13] A. Spek, *ACTA Crystallogr. D* **2009**, *65*, 148-155.
[14] P. Sippel, D. Denysenko, A. Loidl, P. Lunkenheimer, G. Sastre, D. Volkmer, *Adv. Funct. Mater.* **2014**, *24*, 3885-3896.
[15] J. Liu, Y. Liu, N. Liu, Y. Han, X. Zhang, H. Huang, Y. Lifshitz, S.-T. Lee, J. Zhong, Z. Kang, *Science* **2015**, *347*, 970-974.
[16] X. Chang, T. Wang, J. Gong, *Energy Environ. Sci.* **2016**, *9*, 2177-2196.

10.1002/anie.201913284

WILEY-VCH

Entry for the Table of Contents (Please choose one layout)

COMMUNICATION

A series of stable heterometallic Fe_2M cluster-based MOFs achieve the overall conversion of CO_2 and H_2O to HCOOH and O_2 without the assistance of additional sacrificial agent and photosensitizer. This work proposes a new strategy for how to design crystalline photocatalyst to realize artificial photosynthetic overall reaction.

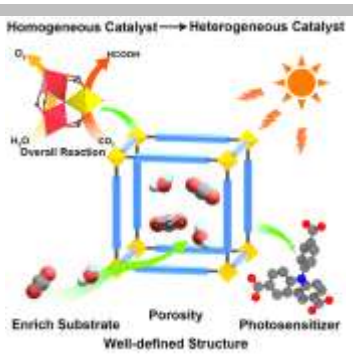

L.-Z. Dong, L. Zhang, J. Liu, Q. Huang, M. Lu, W.-X. Ji and Y.-Q. Lan**

Page No. – Page No.

Stable Heterometallic Cluster-Based Organic Frameworks Catalysts for Artificial Photosynthesis